

# Journal of Materials Chemistry B

Accepted Manuscript



This is an *Accepted Manuscript*, which has been through the Royal Society of Chemistry peer review process and has been accepted for publication.

*Accepted Manuscripts* are published online shortly after acceptance, before technical editing, formatting and proof reading. Using this free service, authors can make their results available to the community, in citable form, before we publish the edited article. We will replace this *Accepted Manuscript* with the edited and formatted *Advance Article* as soon as it is available.

You can find more information about *Accepted Manuscripts* in the [Information for Authors](#).

Please note that technical editing may introduce minor changes to the text and/or graphics, which may alter content. The journal's standard [Terms & Conditions](#) and the [Ethical guidelines](#) still apply. In no event shall the Royal Society of Chemistry be held responsible for any errors or omissions in this *Accepted Manuscript* or any consequences arising from the use of any information it contains.



Journal Name

ARTICLE

## Electron transfer driven highly valent silver for chronic wound treatment

K. Yang,<sup>a</sup> J. Liu, H. G. Shi,<sup>a</sup> W. Zhang,<sup>\*a</sup> W. Qu,<sup>a</sup> G. X. Wang,<sup>a</sup> P. L. Wang,<sup>a</sup> and J. H. Ji<sup>a</sup>

Received 00th January 20xx,  
Accepted 00th January 20xx

DOI: 10.1039/x0xx00000x

www.rsc.org/

Although silver is widely added to various chronic wounds to kill higher concentrations ( $10^7$ - $10^8$  CFU/mL) of bacterial, overdose of silver remains a major cause of diverse side effects, such as cytotoxicity and tissue and organ damages. Here we performed reducing dose level of silver, additionally conferred electron transfer potential, could simultaneously achieve good biocompatibility and strong bactericidal ability without introducing extra chemical residual for chronic wound treatment. A systematic investigations demonstrated 1 ppm trivalent silver ions performed rapid (5min) and effective antibacterial activities against pathogens while not significantly affecting cell viability which were equivalent to 20 ppm monovalent silver ions with cytotoxicity, and accelerated the healing process and improved the tissue quality of burn wounds. The killing effect is independent of material and mainly controlled by electron transfer potentials of trivalent silver ions, which disrupts the electron transport of bacteria membrane respiration and leads to bacterial death. Together, such trivalent silver opens up new possibilities for dispelling concern of silver usage in biosafety and provides an avenue for designing of antibiotics or other biomedical applications.

### 1. Introduction

Chronic wounds from burn, trauma and diabetic ulcer<sup>1-3</sup> are easily infected by bacteria and difficult to heal thoroughly. Silver has traditionally been applied in healthcare, such as antibacterial material for chronic wounds because of broad-spectrum bactericidal performance against drug resistance<sup>4, 5</sup> and fluorescent material for cancer biomarker diagnosis.<sup>6</sup> An ideal treatment of these chronic wounds need dual-functions of preventing bacterial infection and promoting wound healing. However, silver can't simultaneously meet both of these requirements due to high-dose silver,<sup>7</sup> asked for killing the higher bacterial concentration ( $10^7$ - $10^8$  CFU/mL) of wounds, deposits in skin and internal organs<sup>8, 9</sup> and causes diverse side effects to damage the normal cell and tissue physiology.<sup>10, 11</sup> For that reason silver products are widely limited to be used in healthcare area.<sup>12</sup> Herein, it is highly desirable that reducing the dose level of silver keeps strong biocidal activity and good biocompatibility.

From the view of studied object, there is an electron conduit on the basis of respiratory proteins between bacterial membranes and extracellular environment to produce energy for bacterial growth and maintenance.<sup>13-16</sup> The change of electron transfer can perturb bacterial electron transport homeostasis, make bacteria lose energy and quickly die. Inspired by this, the paper presents silver, additionally conferred electron transfer potential, performs rapid and

efficient antibacterial action through targeted interactions with bacteria. The tunability of the electronic properties of silver provides an avenue to induce perturbations of bacterial respiration by simply altering the valence state of silver. It is likely that using the tailored electron transfer potentials of silver can be exploited to potently kill pathogens with reducing dose of silver. More importantly, it is independent of material and no extra chemical residual in the antibacterial process of electron transfer for preventing potential side effects. The main objective of this investigation is to preform that the low-dose trivalent silver complex could desirably achieve dual-functions of good biocompatibility and strong bactericidal ability. Investigation of these effects might dispel customer concerns in biosafety and present an interesting clinical avenue for treatment of chronic wounds.

### 2. Experiment detail and methods

#### 2.1 Materials

Sodium periodate ( $\text{NaIO}_4$ ), sodium persulfate ( $\text{Na}_2\text{S}_2\text{O}_8$ ), sodium hydroxide ( $\text{NaOH}$ ) and silver nitrate ( $\text{AgNO}_3$ ) were obtained from Sigma-Aldrich. The Carbopol® 940 were purchased from Lubrizol. All other chemicals and reagents commercially available were of the highest analytical grade.

#### 2.2 Preparation

The trivalent silver complex was synthesized by conventional thermal chemical reduction method. Briefly, the 5.70 g  $\text{NaOH}$ , 3.24 g  $\text{NaIO}_4$  (ligand) and 200 mL  $\text{H}_2\text{O}$  were heated with vigorous magnetic stirring at 80 °C. Sequentially, the  $\text{Na}_2\text{S}_2\text{O}_8$

<sup>a</sup> Technical Institute of Physics and Chemistry, Chinese Academy of Sciences, Beijing 100190, P.R. China. \*Email: weizhang@mail.ipc.ac.cn, Fax: +86-10-82543776, Tel: +86-10-82543776

(3.00g, oxidant) and  $\text{AgNO}_3$  (1.36g) were added. The reaction kept for 1 h. Then, the supernatant was retained at 0–4 °C for recrystallization. The reaction product was collected the next day, filtered and washed with cold water and dried at 50 °C, finally obtained the orange  $\text{Ag}(\text{III})$  complex  $\text{Na}_5\text{Ag}(\text{IO}_6\text{H})_2 \cdot 8\text{H}_2\text{O}$ .<sup>17</sup>

### 2.3 Methods

**2.3.1 Structure characterization.** The absorption spectra were recorded from a UV-Vis spectrophotometer (Cary 5000, Varian, US) in the wavelength range of 200–900 nm. FTIR spectra were acquired on a FTIR spectrometer (Excalibur 3100, Varian, US). XPS measurements were performed on an X-ray photoelectron spectroscopy (ESCALAB 250XI). The binding energy obtained in the XPS analysis were standardized for specimen charging using carbon (C 1s) as the reference at 285 eV. The data analysis and multi-peak fitting were performed by the XPS Peak Fit software Version 4.1.

**2.3.2 Cyclic voltammetry.** A potentiostat CHI660 with three electrodes was employed for the electrochemical measurements. The Pt electrode was used as working electrode. A standard calomel electrode (SCE) was used as the reference. The electrolyte solution (0.1 M,  $\text{KNO}_3$ ) was deaerated by high purity Argon gas prior to the measurements. For measurement of  $\text{Ag}(\text{III})$  complex electro-oxidation reaction activities, cyclic voltammetry (CV) was performed in a solution containing  $\text{Ag}(\text{III})$  complex at room temperature.

**2.3.3 Bacterial Strains and Culture Conditions.** The test organisms include six strains of Gram-negative bacteria (*E. coli* (ATCC 25922) and *P. aeruginosa* (ATCC 15442)), Gram-positive bacteria (*S. aureus* (ATCC 6538), *Kocuria varians* (AS 1.2156), *Staphylococcus epidermidis* (AS 1.4260) and *Micrococcus varians* (AS 1.523) and fungi (*Monilia albican* (ATCC 10231)). The strains were obtained from American type culture collection (ATCC) and China general microbiological culture collection center (CGMCC). Before each microbiological experiment, all samples and glassware were sterilized by autoclaving at 120 °C for 10 min. Cultures of bacteria were grown according to the national standard. A final bacterial concentration of approximately  $\sim 10^7$ – $10^8$  CFU/mL was prepared in 0.9% saline solution.

**2.3.4 Antibacterial assay.** Minimal inhibitory concentration (MIC) was determined by the lowest concentration which inhibits at least 99% of bacterial growth.<sup>18</sup> The strains were grown in tryptic soy broth at 37 °C. The MICs of the  $\text{Ag}(\text{III})$  complex and  $\text{AgNO}_3$  against bacteria were measured using Agar dilution method according to Technical Standard For disinfection (2.1.8.3). The test was conducted at 37 °C for 24 h or 48 h.

The antibacterial activity of  $\text{Ag}(\text{I})$  (monovalent silver ions) and  $\text{Ag}(\text{III})$  (trivalent silver ions) in short time by plate counting method. 2 mL of bacteria suspension (*E. coli*, *S. aureus*, *Monilia albican* and *P. aeruginosa*) with a concentration of  $10^5$ – $10^6$  CFU/mL was mixed with 18 mL sample suspension (1 ppm, 4 ppm, 20 ppm  $\text{Ag}(\text{I})$  and  $\text{Ag}(\text{III})$ ) and incubated under constant shaking (200 rpm/min). After 5 min and 2 h, the mixture was serially diluted, and 1 mL of each dilution was

dispersed onto PCA (plate count agar) or PDA (potato dextrose agar) growth medium. Survival colonies on plates were counted after incubation at 37 °C for 24 h or 48 h.

The antibacterial stability of  $\text{Ag}(\text{III})$  was measured. The 1 ppm  $\text{Ag}(\text{III})$  was stored at 37 °C. The antibacterial percentages against *S. aureus* ( $10^5$ – $10^6$  CFU/mL) after incubated 5 min were measured every 7 day.

The antibacterial rate was calculated by the following formula:  $(A-B)/A \times 100\%$ , where A is the average number of bacteria on the control sample (CFU) and B is the average number of bacteria on the test samples (CFU).

**2.3.5 In vitro cytotoxicity and cell viability evaluation.** Cell-viability following silver materials was determined by a methyl thiazolyl tetrazolium (MTT) assay.<sup>19</sup> Briefly, cells were plated in 96-well plates with a concentration of  $1 \times 10^4$  L929 cells per well. The cells were then incubated under a fully humidified atmosphere of 95% air and 5%  $\text{CO}_2$  at 37 °C overnight. The next day, the 10  $\mu\text{L}$  samples were added to cell cultures at final concentrations of 20, 4 and 1 ppm. After 24 h of further incubation, MTT (20  $\mu\text{L}$ , 5 mg/mL) was added to each well and the plate was incubated for an additional 4 h at 37 °C under 5%  $\text{CO}_2$  to allow the conversion of MTT into a purple formazan product by active mitochondria. The supernatants were discarded. Subsequently, 200  $\mu\text{L}$  of dimethyl sulfoxide (DMSO) was added to dissolve the formazan crystals, and quantified by the absorbance at 490 nm, which was measured by means of a Tecan Infinite M200 monochromator-based multifunction microplate reader (BIO-RAD iMark™ microplate reader).

**2.3.6 Burn wound model.** All procedures about animal were carried out according to the National Institutes of Health Intramural Animal Use and Care Committee (IACUC-2012-047). Male adult Sprague–Dawley rats, weighing around 250–300 g, were acclimatized for one week before experiments under a 12 h dark/light cycle in a room with controlled temperature and humidity. Standard rat chow and water were supplied ad libitum. Prior to the experiments, rats were anesthetized with an intraperitoneal dose of 1 mL 2% pentobarbital sodium. A full thickness burn wound was made on the shaved dorsum of the anesthetized rats with a 0.8 cm diameter brass cylinder heated in a water bath at 100 °C for 2 min and pressed against the rat skin for 20 s. Immediately following the burn, 20  $\mu\text{L}$   $10^8$  CFU/mL of bacteria (*S. aureus*) was inoculated into four injuries inflicted on each rat ( $n = 6$ ). Here, we took advantage of a commercially available hydrogel, Carbopol®, a vehicle for topical administration that maintains a moist environment within the wound site.<sup>20</sup> After 24 h, about 50 mg of the Carbopol gel, 1 ppm  $\text{Ag}(\text{III})$  gel and 1 ppm  $\text{Ag}(\text{I})$  gel were topically applied to the surface of the wound. Phosphate Buffered Saline (PBS) topically administered using the same regimen was used to evaluate the recovery of the rat burn perse. Wound tissues were collected after the burn was made and at 2 and 21 days for tissue analysis. Normal skin was also collected from an area distant from the burn for comparison. Photographs of the wounds were taken at the same defined time points (0 d, 7 d, 14 d and 21 d) using a digital camera. Wound size was then determined with the

aid of Image J 1.46r software (NIH, USA) until re-epithelialization was achieved.

**2.3.7 Histology evaluation.** For histological analysis, the harvested samples were fixed in 4% formaldehyde in PBS at 4 °C, dehydrated in a graded series of ethanol, and then embedded in paraffin for routine haematoxylin-eosin (H&E) staining for rat skin.

**2.3.8 Statistical analysis.** The data were expressed as means  $\pm$  standard deviations. All data were analyzed by a nonparametric U Mann–Whitney test (IBM SPSS Statistics 20 software, Armonk, NY, USA), and the  $p$  values  $<0.05$  were considered to be statistically significant.

### 3. Results

#### 3.1 Ag(III) complex characterization

Using chemical reduction method obtained the orange Ag(III) complex  $\text{Na}_5\text{Ag}(\text{IO}_6\text{H})_2 \cdot 8\text{H}_2\text{O}$ .<sup>17</sup> Structural confirmation of trivalent silver was conducted by UV-Vis, FTIR and XPS. Structure of bis(hydrogen periodato)argentite(III) complex anion,  $[\text{Ag}(\text{HIO}_6)_2]^{5-}$  have demonstrated by researchers<sup>21</sup>, which contains trivalent silver ions surrounded by four oxygen atoms from two  $\text{IO}_6$  octahedra in rectangular configuration. As shown in Fig. 1a, silver nitrate did not show any significant absorption peaks. A new absorption peak at 361.88 nm appeared, which is assigned to the charge transitions between the central atom and the ligand according to the molecular orbital theory. The absorption peaks observed at around 211.4 nm and 362.0 nm are corresponding to the Ag(III) complex. The shorter wavelength peak at 211.4 nm is assigned to transition of  $\text{IO}_6^{5-}$ , whereas the longer wavelength peak at 362.0 nm corresponds to d-d electronic transitions of Ag(III) complex. The stronger the ligand field of complex, the higher splitting energy of d orbital and the shorter wavelength of absorption peak. The result implied the energy of coordinate bond is larger. Fig. 1b performed FTIR spectra of  $\text{NaIO}_4$  salt which showed the peaks at wavenumbers 3412.1, 1634.6 and  $1382.1 \text{ cm}^{-1}$ .<sup>22</sup> Compared to it, the spectrum of Ag(III) complex shifted to the lower wavenumber (red shift). The result reflected that binding was due to the interaction between the silver and  $\text{IO}_6^{5-}$  bond. The oxidation state of Ag in complex was investigated by Ag 3d XPS. Furthermore, the XPS binding energy is mostly determined by the oxidation state of the studied atom but could also be influenced by its chemical environment. From the measurements of Ag 3d XPS spectra for Ag(III) complex (Fig. 1d), the Ag  $3d_{3/2}$  and Ag  $3d_{5/2}$  XPS peaks were observed at 376.0 and 370.0 eV, respectively, differed from  $\text{AgNO}_3$  (Ag  $3d_{3/2}$ : 368.3 eV; Ag  $3d_{5/2}$ : 374.3 eV) (Fig. 1c),<sup>23</sup> which fall in the range of literature values for  $\text{Ag}^{3+}$ .<sup>24</sup>

Some of the d electrons of the  $\text{Ag}^+$  ion must be forced to occupy higher-energy anti-bonding orbitals, from which they can be removed by peroxydisulfate oxidation to produce a trivalent silver complex. Furthermore, Fig. 2 presented the cyclic voltammograms of Ag(III) complex, which had two main oxidation peaks ( $\text{O}_1$  and  $\text{O}_2$ ) during the anodic scan and two reduction peaks ( $\text{R}_1$  and  $\text{R}_2$ ) during the reversed scan. The first oxidation peak ' $\text{O}_1$ ' observed at about 0.296 V (V vs SCE) and the second oxidation peak ' $\text{O}_2$ ' was observed at about 0.695 V during the anodic scan, which was accompanied by the

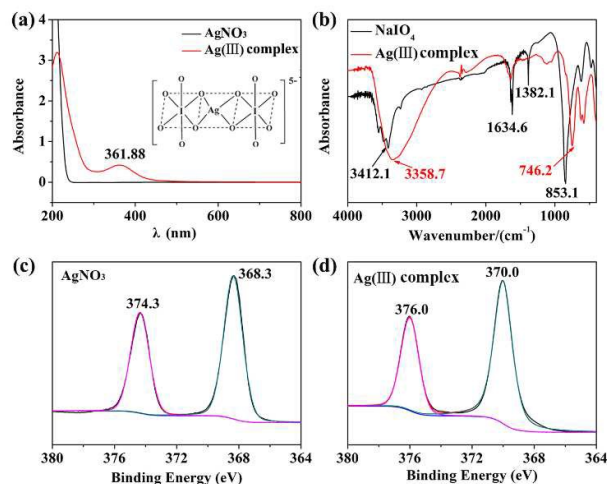


Fig. 1 Structure characterization. (a) UV-Vis absorption spectra of  $\text{AgNO}_3$  (Inset: structure of bis(hydrogen periodato)argentate(III) complex anion,  $[\text{Ag}(\text{HIO}_6)_2]^{5-}$ ) and Ag(III) complex. (b) FTIR spectra of  $\text{NaIO}_4$  and Ag(III) complex. (c-d) XPS spectra of  $\text{AgNO}_3$  and Ag(III) complex.

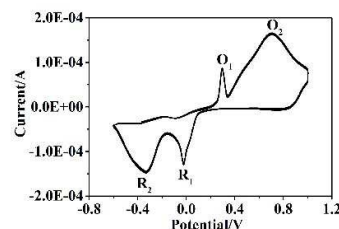


Fig. 2 Cyclic voltammograms of Ag(III) complex in 0.1 M  $\text{KNO}_3$  solution.

appearance of the two reduction peaks during the reversed scan at about -0.022 V and -0.367 V to the two oxidation peaks respectively. The peaks ' $\text{O}_1$ ' and ' $\text{O}_2$ ' corresponded to the formation of  $\text{Ag}^+$  and  $\text{Ag}^{3+}$  respectively and the peaks ' $\text{R}_1$ ' and ' $\text{R}_2$ ' during the reversed scan corresponded to the reduction of  $\text{Ag}^{3+} \rightarrow \text{Ag}^+$  and  $\text{Ag}^+ \rightarrow \text{Ag}$  respectively. The results confirmed that the trivalent silver had higher potential and been conferred electron transfer potential through changing the chemical valence.

#### 3.2 Antibacterial activity and cytotoxicity in vitro

Common bacterial strains in chronic wounds, such as *S. aureus*, *P. aeruginosa* and *E. coli* etc., are used to evaluate the antibacterial properties of Ag(III) complex *in vitro*. Determination of MIC is a microbiological technique used to quantitatively evaluate bactericidal activity against high concentration pathogens. Therefore, the MIC values and growth of colonies for Ag(I) (monovalent silver ions, as control) and Ag(III) (trivalent silver ions) were determined and recorded in Fig. 3, which showed the growth of colonies was performed with different concentrations Ag(I) and Ag(III) against several common bacterial pathogens. The Ag(III) has MICs against *E. coli* of 4 ppm, *Monilia albican* of 2 ppm, and others (*S. aureus*, *P. aeruginosa*, *Kocuria varians*, *Staphylococcus epidermidis* and *Micrococcus varians*) of 8 ppm. The MICs of Ag(I) are 4 ppm against *Monilia albican*, 32 ppm against *P. aeruginosa*, and 16 ppm against others (*E. coli*, *S. aureus*, *Monilia albican*, *Staphylococcus epidermidis* and

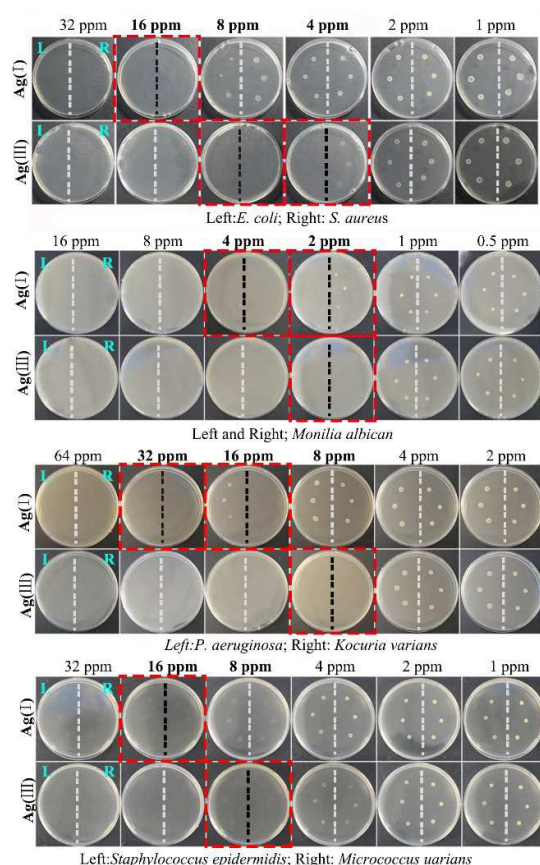


Fig. 3 MIC values via the growth of bacterial colonies with different concentration Ag(I) and Ag(III). Note: "L"/"R" means the left/right of every plate is the same strain.

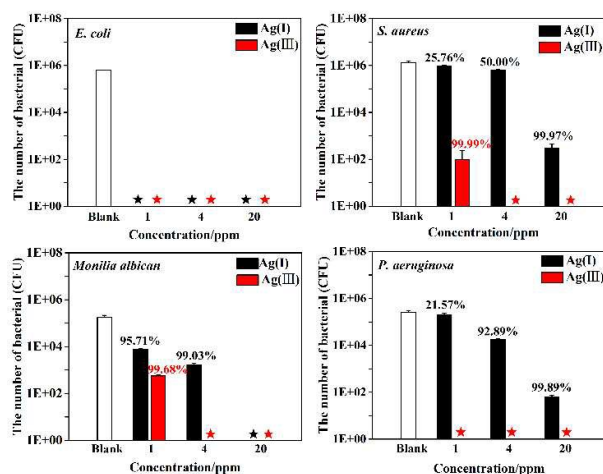


Fig. 4 Antibacterial activity after incubated 5 min against *E. coli*, *S. aureus*, *Monilia albican* and *P. aeruginosa* with blank, Ag(I) and Ag(III) (1 ppm, 4 ppm and 20 ppm). Note: "\*" and "\*" mean the number of bacterial is zero.

*Micrococcus varians*). The MICs of Ag(I) was 2-4 times of Ag(III). Additionally, no antimicrobial effects of the  $\text{NaIO}_4$  and  $\text{Na}_2\text{S}_2\text{O}_8$  (test concentrations  $\leq 128$  ppm) were observed against the bacterial strains tested. From the above observations it is established that the synthesized Ag(III) complex has superior

antibacterial properties against high concentration ( $10^7$ - $10^8$  CFU/mL) both gram-negative and gram-positive bacteria and fungi.

In Fig. 4, the number of surviving bacteria is graphically represented as a function of the Ag(I), Ag(III) samples and a control sample (Blank) after only incubated 5 min against *E. coli*, *S. aureus*, *Monilia albican* and *P. aeruginosa*. For *E. coli*, all Ag(I) and Ag(III) exhibited nearly complete bacterial growth reduction (>99.90%), which indicated that silver was suspicious of *E. coli*; For *S. aureus* and *P. aeruginosa*, the antibacterial percentage of 1 ppm Ag(III) reached more than 99.00%, the antibacterial percentage of 1 ppm Ag(I) was less than 30.00%; For *Monilia albican*, the antibacterial percentages of 1 ppm Ag(I) and Ag(III) were up to 95%. The Fig. 5(a) showed the antibacterial percentages against bacteria in detail. Combined Fig. 4 and Fig. 5(a), the antibacterial activity of the silver ranked as: Ag(I) < Ag(III) (*S. aureus*, *Monilia albican* and *P. aeruginosa*). There is no comparison for bactericidal property against *E. coli* between Ag(III) and Ag(I) in the range of 1 ppm to 20 ppm. It was noted that the same concentration Ag(III) provided faster and more effective antibacterial action, as antibacterial percentage were higher than 99.50% within 5 min after the beginning of the experiment against *S. aureus*, *Monilia albican* and *P. aeruginosa* compared to Ag(I). Most of bacteria in 1 ppm Ag(III) were killed within 5 min. Thus, it implied that the antibacterial mechanism of trivalent silver should be different from that of conventional monovalent silver, which deactivated microorganism cells by interacting with disulfide or sulphydryl groups of the enzymes, and further causing structural changes and destroying the metabolic process of bacterial cells.<sup>25</sup> More than 99.99% of viable colonies were vanished when the contact time was extended up to 2 h (Fig. 5b). Besides, to evaluate the stability of Ag(III) complex, the samples had been tested after incubated 5 min against *S. aureus* ( $\sim 10^6$  CFU/mL) every 7 d in 28 days and their antibacterial activity was further evaluated using the same method (Fig. 5c). The number of surviving bacteria was zero, which indicated that Ag(III) complex had a good stability in antibacterial activity against storage. The results demonstrated the trivalent silver ions enhanced antibacterial property because the bactericidal effect obtained by 1 ppm trivalent silver ions was equivalent to 20 ppm monovalent silver ions, especially against *S. aureus* and *P. aeruginosa*.

In order to evaluate the biocompatibility of Ag(III) samples, L929 cells were employed to characterize cell viability in a dose-dependent manner as determined by MTT assay. The MTT result was illustrated in Fig. 5(d) as relative viability of the cells by comparison with the control well containing only the cells. In the concentrations tested, 1 ppm Ag(III) and Ag(I) revealed a much lower cytotoxic effect to L929 cells, and the L929 viability was over 95%. However, the cell viability of Ag(III) and Ag(I) was 55% and 52% at concentration 20 ppm, 88% and 89% at concentration 4 ppm. No significant difference was noticed between Ag(III) and Ag(I) at the same concentration. Combined Fig. 4 and Fig. 5(d), the results indicated 1 ppm trivalent silver ions elicited rapid and effective

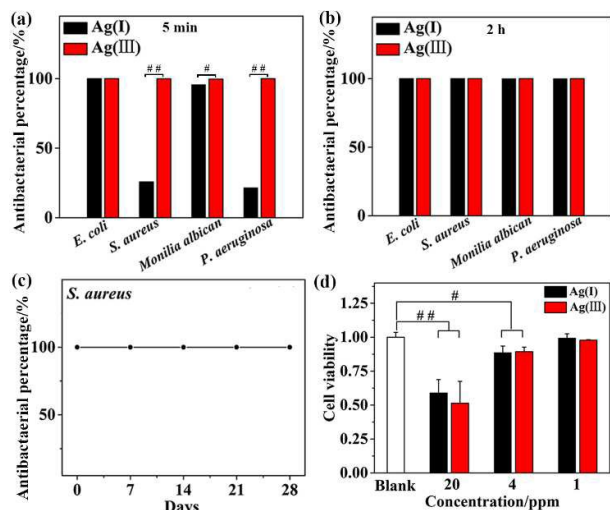


**Fig. 5** The antibacterial activity in different reaction time, antibacterial stability and cell viability. (a–b) The antibacterial percentage after incubated 5 min and 2 h of 1 ppm Ag(I) and 1 ppm Ag(III) against *E. coli*, *S. aureus*, *Monilia albican* and *P. aeruginosa*, respectively. The number of bacteria is zero after incubated 2 h. (c) The antibacterial percentages against *S. aureus* ( $10^5$ – $10^6$  CFU/mL) after incubated 5 min were measured by 1 ppm Ag(III) stored at 37 °C in different periods. The number of bacteria is zero. (d) Cytotoxic effects of different concentration Ag(I) and Ag(III). Note: “#” means  $0.01 < p < 0.05$ ; “##” means  $p < 0.01$ .

bactericidal properties without cytotoxicity, which nearly completed bacterial growth reduction (>99.50%) in 5 min against *S. aureus* and *P. aeruginosa*, especially equivalent to 20 ppm monovalent silver ions with cytotoxicity.

### 3.3 Wound healing

To evaluate the *in vivo* effectiveness of Ag(III) in chronic wounds of an infected burn model, groups of rats were given full-thickness scald burns and then immediately infected with *S. aureus*, which is one of the most commonly isolated species in chronic wounds. According to the Fig. 4 and Fig. 5d results, chosen 1 ppm trivalent silver ions were further embedded in Carbopol®, a commercially available hydrogel, a vehicle for topical administration that maintains a moist environment within the wound site. We applied the PBS (blank control group), Carbopol (negative control group), 1 ppm Ag(I) gel (positive control group) and 1 ppm Ag(III) gel on top of the wounds after bacterial infection. General morphology of the wounds was evaluated over time in the rat burn model.

Macroscopic analysis of the wounds showed the healing progression after the treatments were administered (Fig. 6a). After 7 days, the wounds had formed a hard scar. Between day 7 and day 14, part of the wound scabs began to fall, especially Ag(III) and Ag(I) gels. A faster reduction in wound size was observed in the presence of Ag(III) and Ag(I) gel, particularly up to day 21. After 21 days full wound closure was basically attained for treatments. In accordance with the qualitative analysis (Fig. 6b left), quantitative evaluation of wound closure showed that the Ag(III) accelerated the wound healing process, as a significant decrease in wound area was observed at days 14 and 21, in comparison with Ag(I). Additionally, we could visually see the changes in the size of

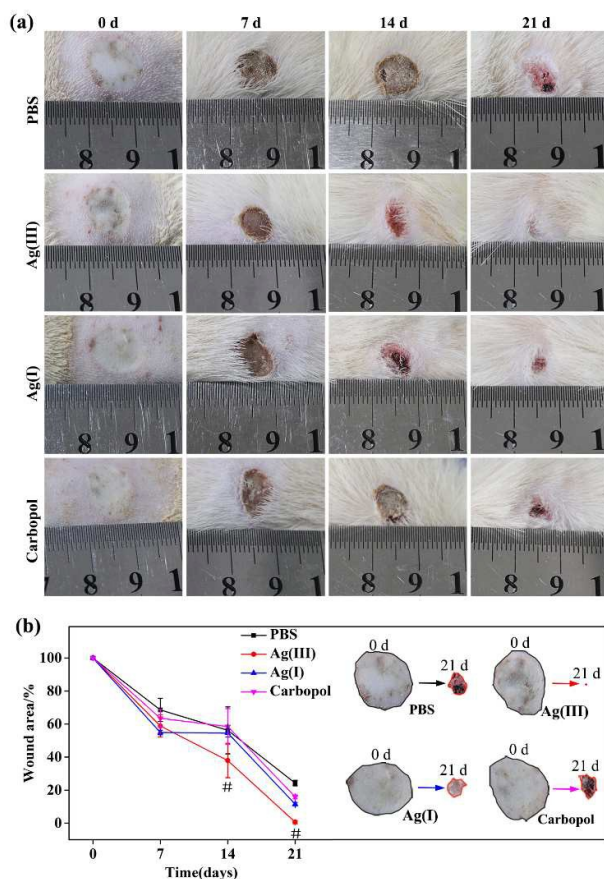


**Fig. 6** Treatment of rat burn wounds with samples. (a) Macroscopic changes in wound size over time after treatment with the Ag(III) in comparison with the Ag(I) alone. (b) Percentage of wound closure over time after wound tracing and Image J analysis (left). Data in the graph represent the mean  $\pm$  S.D. for an  $n = 6$ . The changes of wound area from 0 d to 21 d (right).

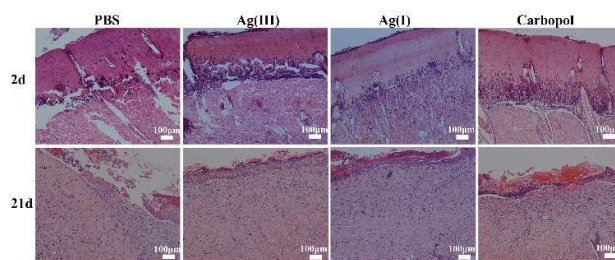


**Fig. 7** Histological evaluation of burn wound cross-sections. Tissues from day 2 and 21 post-injury were stained using H&E. The bar corresponds to 100  $\mu$ m.

the wound from 0 d to 21 d (Fig. 6b right) and the wound healed completely with Ag(III) treatment. As illustrated in Fig. 6, the situations of wound closure showed that the Ag(III) accelerated the wound healing process, as a significant decrease in wound area was observed at days 14 and 21, in comparison with other wounds.

### 3.4 Histological observation

Histological analyses of dorsal skin lesions stained with H&E were visible in the magnified image (Fig. 7). The structural integrity of the tissue was significantly altered, giving rise to

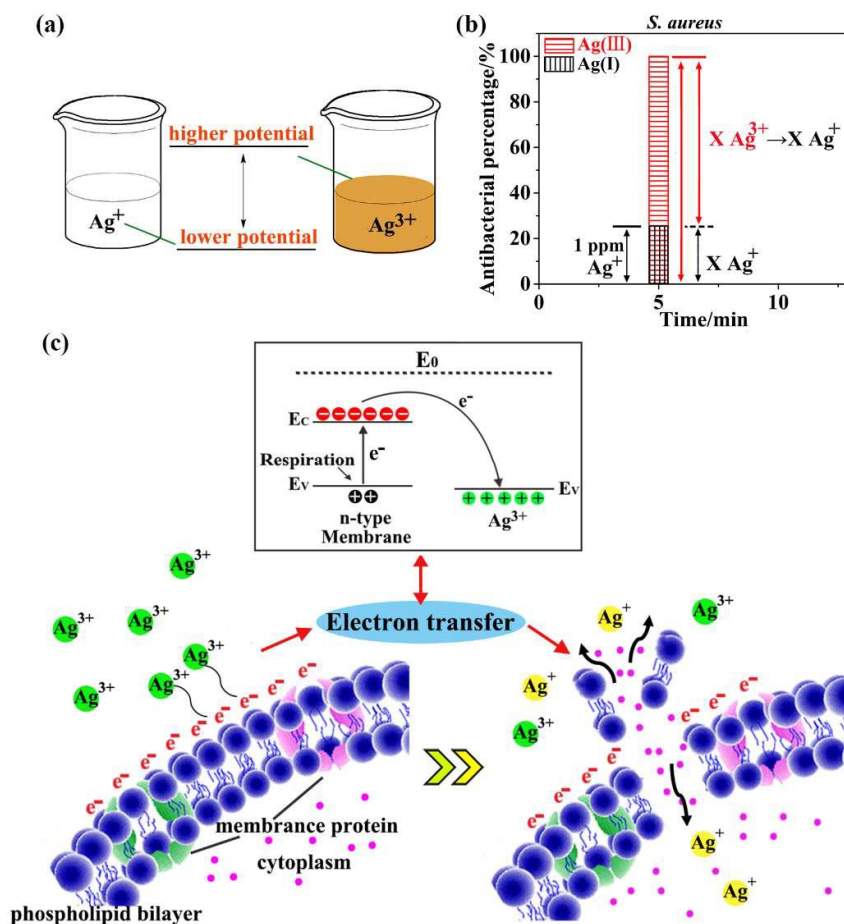


Fig.8 (a) Schematic illustrating the potentials of  $\text{Ag}^+$  and  $\text{Ag}^{3+}$ ; (b) the comparison of antibacterial percentage between 1 ppm  $\text{Ag(I)}$  and 1 ppm  $\text{Ag(III)}$  after incubated 5 min against *S. aureus* ( $0 < X \leq 1$ ); (c) one hypothetical antibacterial mechanism of  $\text{Ag(III)}$  complex. Notes:  $E_0$ , vacuum level;  $E_c$ , conduction band.

more disorganized extracellular matrix, loss of hair-shaft follicles in the dermis, and detachment of the epidermis in most specimens. There was also extensive lymphocyte infiltration at the interface of injured and healthy tissue. At day 2, infected burns treated with PBS,  $\text{Ag(III)}$ ,  $\text{Ag(I)}$  and Carbopol did exhibit severe inflammatory tissue response. All of infected burns exhibited oedema and severe inflammation. Typical infiltration of granulocytes was observed in all groups, and macrophages were also observed at this stage. The lymphocytes were present in all group. At day 21, the oedema is basically disappeared. However, blood vessels were present in A and D groups, which is consistent with the results in Fig. 6. After day 21, the  $\text{Ag(III)}$  gel showed the wound basically healed, intercellular substance increased and epidermis completely covered the wound, which was better than  $\text{Ag(I)}$  gel.<sup>26</sup>

#### 4. Discussion

Amongst the wide range of studies on metals with antimicrobial activity, silver has attracted the attention

because of its highly antimicrobial potential against drug-resistant microorganisms<sup>5, 27, 28</sup>. However, the dose of silver ions is closely related with antimicrobial property and biocompatibility. Overdose of silver poses a significant practical problem, causing negative side effects in the healthcare. Hence, it is highly desired to control the actions of silver to bacterial and mammalian cells to kill pathogenic microbes while simultaneously avoiding toxicity to cells. In order to overcome these drawbacks, an attempt is made to improve the valence of silver inspired by electron transfer, which has the potential to disrupt the electron transport of bacteria membrane respiration to provide energy for vital movements and lead to bacterial death<sup>29</sup>, accordingly achieving good biocompatibility and strong bactericidal ability.

Firstly, the  $\text{Ag(III)}$  complex (Fig. 8a) was prepared by chemical reduction method using  $\text{S}_2\text{O}_8^{2-}$  as oxidant and  $\text{IO}_6^{5-}$  as ligand, which was fabricated using the following reaction:  $\text{Ag}^+ + \text{IO}_6^{5-} + \text{S}_2\text{O}_8^{2-} + \text{OH}^- \rightarrow [\text{Ag}(\text{IO}_6\text{H})]^{2+} + \text{SO}_4^{2-} + \text{H}_2\text{O}$ .<sup>17</sup> As expected, the trivalent silver formation was conclusively demonstrated with the peaks of  $\text{Ag } 3d_{3/2}$  (376.0 eV) and  $\text{Ag } 3d_{5/2}$  (370.0 eV) XPS peaks by XPS analysis (Fig. 1d), which differed from

monovalent silver (Fig. 1c). The UV-Vis spectra (Fig. 1a) of the fabricated Ag(III) confirmed the complex exists because of additional peak at 362.0 eV. When the central atom is high oxidation state, it is happened the charge transitions from the ligand to the central metal atom (LMCT). Simultaneously, the FTIR spectra of Ag(III) complex revealed a pronounced shift to lower wavenumbers (red shift) than that of  $\text{NaIO}_4$  (Fig. 1b), attributed to the ligand ( $\text{IO}_6^{5-}$ ) give electrons the central metal atom ( $\text{Ag}^{3+}$ ). Furthermore, the trivalent silver ions were conferred electron transfer potential (Fig. 2) and had higher potential (Fig. 8a), which extremely eagered to get electrons forming monovalent silver ions directly.

The physicochemical change had a significant impact on the antibacterial properties of synthesized Ag(III) complex. Based on the previous report, the monovalent silver ion have a broad spectrum of pathogens, including gram-positive and gram-negative bacteria and fungi, applied in human clinical applications.<sup>30</sup> Herein, monovalent silver ions are used as a control in order to better reflect the characteristics of the trivalent silver ions. The MIC results (Fig. 3) of Ag(I) and Ag(III) illustrated that the Ag(III) exhibited excellent antimicrobial activities against the seven kinds of common bacteria and fungi. It could be concluded that the dose of Ag(III) is less than Ag(I) to achieve the same antimicrobial effect. Furthermore, it has been demonstrated that the concentrations of silver ions are critical to its antibacterial effects (Fig. 4) and cytotoxicity (Fig. 5). Generally, the cytotoxic effect of silver on mammalian cells may be significantly lower than its antibacterial effect on bacterial cells because eukaryotic cells are usually much larger than prokaryotic cells. In that sense, silver is sufficient to destruct bacterial cells without inducing notable cytotoxicity. According to Fig. 5d and Fig. 4, the toxic effect of silver ions appears at high dose 20 ppm and 20 ppm Ag(I) and Ag(III) could kill all of bacterial. The 4 ppm Ag(I) or Ag(III) displayed lower toxic (Fig. 5d) compared with blank, which were no significant difference. However, the strain of *S. aureus* had 50% and 100% growth inhibition (Fig. 4b) treated with 4 ppm Ag(I) and 4 ppm Ag(III), respectively. The 4 ppm Ag(III) showed better antibacterial activity than Ag(I) in 5 min, particularly the phenomenon was more obvious in 1 ppm concentration against *S. aureus* and *P. aeruginosa*. They were in accordance with our expectations that lower dose Ag(III) exerted rapid and efficient antibacterial performances with good biocompatibility. This is due to the fact that electron transfer happens when trivalent silver ions directly contact with bacterial membrane to disrupt respiration for killing bacteria, yet it is not much effect on most eukaryotic cell whose respiration occurs in mitochondria. In addition, previous reports showed that the dorsal skin of rats was fragile after burn injury, thereby making the damaged skin particularly susceptible to infection by *S. aureus*, which causes systemic inflammation. Therefore, a rat full thickness burn infection model was used to evaluate the antimicrobial properties of the Ag(III) complex. Wound healing processes and neotissue formation were evaluated *in vivo* by macroscopic observations (Fig. 6) and H&E staining (Fig. 7) at

the indicated time points because wound healing is a complex process. At all same time points, the Ag(III) group exhibited a complete glandular cavity, thickened epidermis, granular tissue formation, and big rete pegs as well as keratinocyte restoration, which would be favorable to skin repair. Based on above results, 1 ppm trivalent silver ions embodied good biocompatibility, strong bactericidal ability, and improved and accelerated burn wound-healing, superior to 1 ppm monovalent silver ions.

To the best of our knowledge, the mechanism of monovalent silver ions has been researched.<sup>31, 32</sup> Monovalent silver ions interact with sulfhydryl groups on the surface protein of microorganisms, resulting in inactivation of the bacterial proteins and de-energizing of the membrane and ultimately leading to cell death. Inside the cell, Ag(I) ions also make the cell death because of interacting with DNA, proteins and inducing ROS (reactive oxygen species) production. Currently, no reports have conclusively documented the mechanism underlying the antibacterial activity of trivalent silver ions. Combined mentioned above experiments, it may be a logical conclusion considering that rapid bactericidal reaction is happened between trivalent silver ions and bacteria. As shown in Fig. 5(a), the antibacterial percentages of 1 ppm Ag(I) and 1 ppm Ag(III) are 25.76% and 99.99% after incubated 5 min against *S. aureus*, respectively. Therefore, The electron transfer played a major role in bactericidal process because the antibacterial percentage was at least 74.23% when we assumed X ppm Ag(III) ( $0 < X \leq 1$ ) converted to X ppm Ag(I) (Fig. 8b). Furthermore, A schematic circuitry is depicted in Fig. 8c for the contact of microbes and Ag(III). It is well known bacteria carry out respiration to produce energy for survive,<sup>33</sup> which requires extracellular electron acceptors to realize electron transport between the microbial membrane and the extracellular environment.<sup>13, 14</sup> The membranes of bacterial are negatively charged in culturing medium ( $\text{pH}=7.0-7.5$ ) because the isoelectric point value is 2-5.<sup>34</sup> Here we hypothesized that the respiratory proteins may behave as n-type semiconductors because these respiratory proteins may possess semiconductivity with a bandgap of 2.6 eV to 3.1 eV<sup>29</sup> and the ground serves as a reference of zero potential. As illustrated in Fig. 8c, the Ag(III) trapped electron of bacterial surface, happened electron transfer, disrupted the electron transport of bacteria membrane respiration, and directly and quickly lead to bacterial death. Electron transfer is an initial crucial step that determine the interaction between Ag(III) and bacteria. The process of electron transfer can lead to oxidative damage and a variety of biological effects, which was recognized as the main intermediates responsible for antibacterial activity.<sup>35</sup> Additionally, the generated monovalent silver ions also play a certain antibacterial effect and sustain long-term antibacterial property. While the superior antibacterial activity of Ag(III) cannot be explained unambiguously with the present data set and the exact mechanism needs further investigation, this probably reveals the peculiar role of high-valence cation that are efficiently

dissolved in the solution where bacteria are growing, opening an avenue for increased bioavailability of active silver.

## 5. Conclusions

In summary, we developed a new idea to improve the valence state of silver conferred electron transfer potential for keeping good biocompatibility and strong antimicrobial performances. The results indicated the 1 ppm trivalent silver ions elicited rapid and effective bactericidal properties while not significantly affecting cell viability, which nearly were tailored to kill 99.5% of bacterial cells (*S. aureus* and *P. aeruginosa*) in 5 min, especially equivalent to 20 ppm monovalent silver ions with cytotoxicity. Meanwhile, 1 ppm trivalent silver ions improved and accelerated burn wound-healing in a rat full thickness burn infection model. From the viewpoint of charge transfer, the trivalent silver ions disrupted the electron transport of bacteria membrane respiration and then microbe death. Thus, our current findings might address the plight of use in the monovalent silver ion and implicate in the design of novel antibiotics for clinical application.

## Acknowledgements

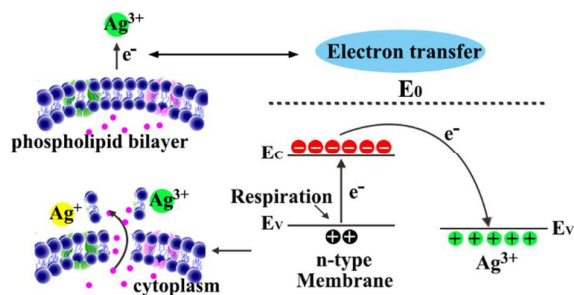
This work is jointly supported by the National Natural Science Foundation of China (NSFC 51473175), National key research and development program (2016YFC1000900) and Youth Innovation Promotion Association CAS.

## References

1. S. Pal, E. J. Yoon, S. H. Park, E. C. Choi and J. M. Song, *J. Antimicrob. Chemother.*, 2010, **65**, 2134-2140.
2. S. Silver, L. T. Phung and G. Silver, *J. Ind. Microbiol. Biot.*, 2006, **33**, 627-634.
3. S. Pal, E. J. Yoon, Y. K. Tak, E. C. Choi and J. M. Song, *J. Am. Chem. Soc.*, 2009, **131**, 16147-16155.
4. R. van Grieken, J. Marugán, C. Sordo, P. Martínez and C. Pablos, *Appl. Catal. B: Environ.*, 2009, **93**, 112-118.
5. S. Chernousova and M. Epple, *Angew. Chem. Inter. Edit.*, 2013, **52**, 1636-1653.
6. H. Pei, S. Zhu, M. Yang, R. Kong, Y. Zheng and F. Qu, *Biosens. Bioelectron.*, 2015, **74**, 909-914.
7. P. Taylor, A. Ussher and R. Burrell, *Biomaterials*, 2005, **26**, 7221-7229.
8. M. Kempf, R. M. Kimble and L. Cuttle, *Burns*, 2011, **37**, 994-1000.
9. S. B. Zou, W. Y. Yoon, S. K. Han, S. H. Jeong, Z. J. Cui and W. K. Kim, *Int. Wound J.*, 2013, **10**, 306-312.
10. Z. M. Davoudi, A. E. Kandjani, A. I. Bhatt, I. L. Kyratzis, A. P. O'Mullane and V. Bansal, *Adv. Funct. Mater.*, 2014, **24**, 1047-1053.
11. S. Eckhardt, P. S. Brunetto, J. Gagnon, M. Priebe, B. Giese and K. M. Fromm, *Chem. Rev.*, 2013, **113**, 4708-4754.
12. B. P. Colman, C. L. Arnaout, S. Anciaux, C. K. Gunsch, M. F. Hochella Jr, B. Kim, G. V. Lowry, B. M. McGill, B. C. Reinsch and C. J. Richardson, *PLoS One*, 2013, **8**, e57189.
13. R. S. Hartshorne, C. L. Reardon, D. Ross, J. Nuester, T. A. Clarke, A. J. Gates, P. C. Mills, J. K. Fredrickson, J. M. Zachara and L. Shi, *P. Natl. Acad. Sci.*, 2009, **106**, 22169-22174.
14. H. W. Harris, M. Y. El-Naggar, O. Bretschger, M. J. Ward, M. F. Romine, A. Obratzsova and K. H. Neilson, *P. Natl. Acad. Sci.*, 2010, **107**, 326-331.
15. G. Reguera, K. D. McCarthy, T. Mehta, J. S. Nicoll, M. T. Tuominen and D. R. Lovley, *Nature*, 2005, **435**, 1098-1101.
16. R. Masse and A. Simon, *J. Solid State Chem.*, 1982, **44**, 201-207.
17. Y. Wu, N. Zhou, W. Li, H. Gu, Y. Fan and J. Yuan, *Mat. Sci. Eng. C-Mater.*, 2013, **33**, 752-757.
18. S. Barua, R. Konwarh, S. S. Bhattacharya, P. Das, K. S. P. Devi, T. K. Maiti, M. Mandal and N. Karak, *Colloid Surface B*, 2013, **105**, 37-42.
19. J. P. Silva, S. Dhall, M. Garcia, A. Chan, C. Costa, M. Gama and M. Martins-Green, *Acta Biomater.*, 2015, **26**, 249-262.
20. A. Babapour, B. Yang, S. Bahang and W. Cao, *Nanotechnology*, 2011, **22**, 155602.
21. X. Xu, H. Zhang, H. Shi, C. Ma, B. Cong and W. Kang, *Anal. Biochem.*, 2012, **427**, 10-17.
22. C. V. S. Reddy, Q.Y. Zhu, L.Q. Mai and W. Chen, *J. Appl. Electrochem.*, 2006, **36**, 1051-1056.
23. A. Babapour, B. Yang, S. Bahang and W. Cao, *Nanotechnology*, 2011, **22**.
24. C. Brückner, C. A. Barta, R. P. Brinas and J. A. Krause Bauer, *Inorg. Chem.*, 2003, **42**, 1673-1680.
25. Y. Matsumura, K. Yoshikata, S.-i. Kunisaki and T. Tsuchido, *Appl. Environ. Microb.*, 2003, **69**, 4278-4281.
26. A. F. de Faria, F. Perreault, E. Shaulsky, L. H. A. Chavez and M. Elimelech, *Acs Appl. Mater. Inter.*, 2015, **7**, 12751-12759.
27. D. M. Mitrano, E. Rimmele, A. Wichser, R. Erni, M. Height and B. Nowack, *Acs Nano*, 2014, **8**, 7208-7219.
28. A. Ivask, A. ElBadawy, C. Kaweeteerawat, D. Boren, H. Fischer, Z. X. Ji, C. H. Chang, R. Liu, T. Tolaymat, D. Telesca, J. I. Zink, Y. Cohen, P. A. Holden and H. A. Godwin, *Acs Nano*, 2014, **8**, 374-386.
29. D. Eley and D. Spivey, *Transactions of the faraday society*, 1960, **56**, 1432-1442.
30. W. K. Jung, H. C. Koo, K. W. Kim, S. Shin, S. H. Kim and Y. H. Park, *Appl. Environ. Microb.*, 2008, **74**, 2171-2178.
31. P. Dallas, V. K. Sharma and R. Zboril, *Adv. Colloid Interfac.*, 2011, **166**, 119-135.
32. D. M. Eby, N. M. Schaeublin, K. E. Farrington, S. M. Hussain and G. R. Johnson, *Acs Nano*, 2009, **3**, 984-994.
33. B. A. Haddock and C. W. Jones, *Bacteriological Reviews*, 1977, **41**, 47.
34. V. P. Harden and J. O. Harris, *J. Bacteriol.*, 1953, **65**, 198.
35. R. A. Palominos, M. A. Mondaca, A. Giraldo, G. Peñuela, M. Pérez-Moya and H. D. Mansilla, *Catal. Today*, 2009, **144**, 100-105.

## Highly valent silver with electron transfer potential for chronic wound treatment

Kun Yang,<sup>a</sup> Jun Liu,<sup>a</sup> Haigang Shi,<sup>a</sup> Wei Zhang,<sup>\*a</sup> Wei Qu,<sup>a</sup> Gexia Wang,<sup>a</sup> Pingli Wang<sup>a</sup> and Junhui Ji<sup>a</sup>



This paper performs reducing dose of silver, additionally conferred electron transfer potential, could simultaneously achieve good biocompatibility and strong bactericidal ability without introducing extra chemical residual for chronic wound treatment.